Difference in magnetotail variations between intense and weak substorms

Y. Miyashita,[1] Y. Kamide,[1] S. Machida,[2] K. Liou,[3] T. Mukai,[4] Y. Saito,[4] A. Ieda,[1] C.-I. Meng,[3] and G. K. Parks[5]

Received 18 May 2004; revised 5 August 2004; accepted 24 August 2004; published 3 November 2004.

[1] Using Geotail plasma and magnetic field data, we have statistically studied the difference in substorm-associated magnetotail variations between intense and weak substorms. It was found that for intense substorms the plasmoid-related southward magnetic field and the first decrease in the total pressure occur closer to the Earth. This finding indicates that the magnetic reconnection site at expansion onset is located closer to the Earth in intense substorms, which is consistent with the dependence of the onset latitude in the ionosphere on the substorm intensity. Also, magnetic field lines during the growth phase especially earthward of the magnetic reconnection site are more stretched in intense substorms than in weak substorms. The dipolarization at $X \sim -10\ R_E$ is more significant in intense substorms. Furthermore, the Poynting flux in the lobe toward the plasma sheet and the total pressure during the growth and expansion phases are larger at $X \sim -10\ R_E$ than at larger distances, and they are larger in intense substorms than in weak substorms. The enhancement of the Poynting flux and the decrease in the total pressure associated with expansion onset are also more pronounced at $X \sim -10\ R_E$ in intense substorms. These results suggest that more energy is accumulated and subsequently dissipated in the near-Earth magnetotail at $X \sim -10\ R_E$ during intense substorms. *INDEX TERMS:* 2788 Magnetospheric Physics: Storms and substorms; 2744 Magnetospheric Physics: Magnetotail; 2740 Magnetospheric Physics: Magnetospheric configuration and dynamics; 7835 Space Plasma Physics: Magnetic reconnection; *KEYWORDS:* Geotail, substorm intensity

Citation: Miyashita, Y., Y. Kamide, S. Machida, K. Liou, T. Mukai, Y. Saito, A. Ieda, C.-I. Meng, and G. K. Parks (2004), Difference in magnetotail variations between intense and weak substorms, *J. Geophys. Res.*, *109*, A11205, doi:10.1029/2004JA010588.

1. Introduction

[2] One of the main unsolved issues in magnetospheric physics is the triggering mechanism of the expansion onset of substorms. A number of working models have been put forward, among which the near-Earth neutral line (NENL) model [e.g., *Hones*, 1976; *Baker et al.*, 1996] and the current disruption (CD) model [e.g., *Lui*, 1996] are thought to be the principal candidates. In the CD model, it is proposed that some instability [e.g., *Roux et al.*, 1991; *Lui et al.*, 1990] causes current disruption at $X \sim -10\ R_E$, leading to the so-called dipolarization and the current wedge formation. The region of current disruption expands tailward in the course of a substorm. On the other hand, the NENL model assumes that the magnetic reconnection occurs in the region of $-20 > X > -30\ R_E$, producing the tailward moving plasmoid and the earthward bursty bulk flow. They transport magnetic flux, mass, and energy at a high speed.

[3] Extensive statistical studies have obtained an average picture for the magnetotail variations associated with expansion onset of substorms [e.g., *Baumjohann et al.*, 1991, 1999; *Nagai et al.*, 1998; *Lui et al.*, 1998; *Machida et al.*, 1999; *Miyashita et al.*, 2000, 2003b]. This picture helps us to understand which process triggers the expansion onset. Most of these studies indicated that the magnetic reconnection plays an important and critical role in the substorm triggering. In particular, examining substorm-associated evolution of the three-dimensional structure of the magnetotail, *Miyashita et al.* [2000, 2003b] revealed that the magnetic reconnection first occurs in the premidnight tail at $X \sim -20\ R_E$ a few minutes before expansion onset, and then the dipolarization occurs at $X \sim -10\ R_E$ immediately after expansion onset, simultaneously with substantial evolution of the plasmoid at $X \sim -30\ R_E$.

[4] Another important, but less focused, problem in substorm research is what determines the intensity of substorms. One of the reasons for the importance is that understanding what determines the substorm intensity will

[1]Solar-Terrestrial Environment Laboratory, Nagoya University, Toyokawa, Aichi, Japan.
[2]Department of Geophysics, Kyoto University, Kyoto, Japan.
[3]Johns Hopkins University, Applied Physics Laboratory, Laurel, Maryland, USA.
[4]Institute of Space and Astronautical Science, Japan Aerospace Exploration Agency, Sagamihara, Kanagawa, Japan.
[5]Space Sciences Laboratory, University of California, Berkeley, California, USA.

0148-0227/04/2004JA010588$09.00

lead to providing crucial controlling factors for triggering and subsequent development of substorms [*Lui*, 1993]. Except for a few studies [e.g., *Kokubun and McPherron*, 1981; *Lopez and von Rosenvinge*, 1993; *Yamaguchi et al.*, 2004], most previous studies of magnetotail variations in substorms have not systematically paid much attention to the substorm intensity. In fact, the previous statistical studies of magnetotail variations mentioned above did not consider different levels of the substorm intensity, although they obtained the average picture.

[5] The substorm intensity has different levels from less than 10^5 A to more than 10^6 A in terms of the total current intensity of the auroral electrojet [*Kamide and Akasofu*, 1974]. The energy dissipated as Joule heating in the ionosphere differs by an order of magnitude between weak and intense substorms. The latitude of expansion onset in the ionosphere varies rather systematically with the substorm intensity from >70° to <65°, i.e., more intense substorms take place at lower latitudes [*Kamide and Akasofu*, 1974]. Thus, corresponding to the wide variability of the dissipated energy and the onset latitude in the ionosphere, a similar variability can be expected to exist in the magnetospheric dynamics associated with substorms as well. For example, the locations of the magnetic reconnection and the dipolarization in the magnetotail, which are related to substorm expansion onsets, would depend on the substorm intensity [*Kamide*, 2001].

[6] In the present study, we have statistically examined the difference in magnetotail variations and the onset location between intense and weak substorms. For this purpose we used Geotail data extensively. Superposed epoch analyses similar to *Miyashita et al.* [2003b] were performed on the basis of their substorm events.

2. Data and Procedures

[7] We utilized a total of 397 substorm events that occurred during the period from March 1996 to December 1999, which were already chosen by *Miyashita et al.* [2003b]. These events were identified from Polar UVI data [*Torr et al.*, 1995] according to auroral breakups [cf. *Liou et al.*, 1999, 2000]. The substorm expansion onsets (t = 0) were determined with an uncertainty of less than 2 min in timing. In the case of a multiple onset event, we selected not only the first onset but also the second and third (if any) onsets. The events occurred when Geotail was located in the magnetotail region of $-5 \geq X \geq -31\ R_E$ and $|Y| \leq 15\ R_E$ in GSM coordinates.

[8] We classified the 397 substorm events into two groups: intense and weak substorms. How to monitor the substorm intensity is another issue. *McPherron and Baker* [1993] and *Lui* [1993] evaluated various ionospheric and magnetospheric parameters, such as the auroral electrojet indices, the total current in the westward auroral electrojet, the latitude of initial brightening, the amount of precipitating particles, the area of bright auroras, the maximum poleward advance of the auroral bulge, and the duration of auroral activities. In the present study, we adopted the magnitude of positive bays at low and middle latitudes as a measure of the substorm intensity. It was shown that these bays represent an integrated effect of all the current elements in the current wedge including the westward auroral electrojet [*Kamide et al.*, 1974], thus overcoming the insufficient ability of the *AE* indices due to the lack of full coverage of the standard *AE* stations.

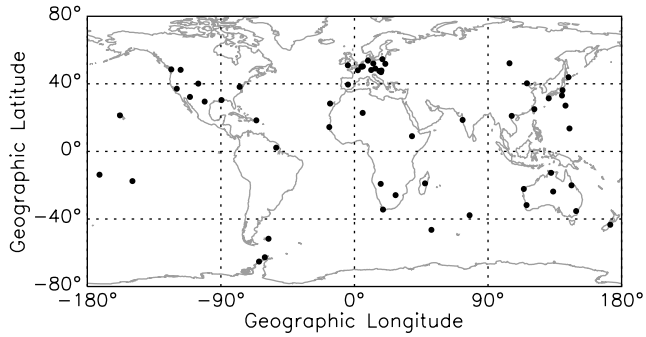

Figure 1. The locations of 58 ground stations whose geomagnetic data were used in the present study. The geomagnetic latitudes of the stations cover the range from 5° to 55°.

[9] For each event, we picked the largest substorm-associated deviation of the north-south (H) component at ground stations which were located at 5°–55° in magnetic latitude and at 19–5 hours in magnetic local time. The locations of 58 ground stations used in the present study are shown in Figure 1. Here, since the magnitude of the positive bay depends on the latitude, i.e., the magnitude at midlatitudes is larger than that at low latitudes by a factor of ~2–3, the deviations were normalized to equatorial values, using the electrojet model 3 of *Kamide* [1970]. Consequently the numbers of intense and weak substorm events are 195 and 202, respectively, where we chose the normalized magnitude of 5.4 nT as the threshold value separating the two groups, making the sample numbers nearly equal. We also performed the same analyses of magnetotail variations, adopting the magnitude of the westward electrojet at high latitudes as a measure of the substorm intensity. However, the magnitudes of the westward electrojet and the positive bay were statistically correlated, thus obtaining basically the same results (not shown here).

[10] Then we statistically obtained the difference in magnetotail variations associated with substorm expansion onset between the two groups, using ion moments and magnetic field data from the Geotail spacecraft. The ion moments such as the number density, the temperature, and the velocity were obtained from the low-energy particle experiment (LEP) [*Mukai et al.*, 1994] and were calculated from the ions with the energy-per-charge range from a few tens of eV/q to ~40 keV/q under the assumption that all ions are protons. The magnetic field was measured by the fluxgate magnetometer of the magnetic field experiment (MGF) [*Kokubun et al.*, 1994]. The time resolution of these data is 12 s, which corresponds to a four-spin period.

3. Superposed Epoch Analyses

[11] Using the Geotail data, we performed superposed epoch analyses for various parameters such as the plasma flow, the north-south magnetic field, the dawn-dusk electric field, the total pressure, and the mass and energy fluxes. These parameters are fundamental to understanding the magnetotail dynamics and the mass and energy transport,

but we show only the results of the plasma flow, the north-south magnetic field, the total pressure, and the energy fluxes in the present paper. The data were averaged in 2 min intervals from 11 min before expansion onset to 11 min after expansion onset for each substorm. The classification of the data into the plasma sheet (PS), the plasma sheet boundary layer (PSBL), and the lobe was based on the definition adopted by *Miyashita et al.* [2000]: the boundary value of the ion β ($=NkT/(B^2/2\mu_0)$) between the PS and the PSBL, β_1, was defined as $\beta_1 = 1$ at $X \leq -15\ R_E$, and $\log_{10}\beta_1 = -0.14X - 2.1$ at $X > -15\ R_E$, and that between the PSBL and the lobe, β_2, was defined as $\beta_2 = 0.05$ at $X \leq -15\ R_E$, and $\log_{10}\beta_2 = -0.14X - 3.4$ at $X > -15\ R_E$, that is, $\beta \geq \beta_1$ for the PS, $\beta_2 \leq \beta < \beta_1$ for the PSBL, and $\beta < \beta_2$ for the lobe.

3.1. Plasma Flow

[12] Figure 2 shows variations in the plasma (ion) flows at different Geotail locations in the PS and PSBL from 6 min before onset ($t = -6$ min) to 6 min after onset ($t = 6$ min) for intense and weak substorms separately. The data of the PSBL are included in the plots, since the PSBL may have characteristics of both the PS and the lobe according to our definition. All flow vectors are plotted even if they are small. Figure 3 shows a sequential plot of the X-directional profile of the X component of the plasma flow (V_x) in the PS and PSBL of $X \leq -5\ R_E$ and $-3 \leq Y \leq 12\ R_E$. The asymmetric Y range with respect to the midnight is due to the dawn-dusk asymmetry of the substorm-associated variations, as shown in the two-dimensional plots of Figures 2 and 4 [see also, e.g., *Nagai et al.*, 1998; *Ieda et al.*, 1998].

[13] As shown in Figure 2, for both intense and weak substorms, there are some fast earthward and tailward flows at a speed of >300 km/s before onset ($t \leq -2 \pm 1$ min). Since the substorm onsets selected in this study include both the first and second onsets, some flows before onset are likely associated with previous auroral breakups or pseudo-breakups. Note also that some earthward flows may come from the distant tail.

[14] It is seen that at onset, fast tailward flows begin to grow significantly in the premidnight sector of $-22 > X > -30\ R_E$ in conjunction with the formation and evolution of the plasmoid. This location is not very different between the two groups, probably because the very thin plasma sheet extends to $X \sim -22\ R_E$ for both intense and weak substorms. On the other hand, only a few earthward flows appear immediately after onset in $-15 > X > -30\ R_E$ as well as at $X \sim -10\ R_E$, probably due to the very thin plasma sheet and the localization of the flows in the Y direction.

[15] Comparing the plasma flows for intense and weak substorms, the location and timing of the first development of the fast flows do not differ very much between the two groups. While a clear difference in the speed of the earthward flow cannot be identified, the tailward flow for intense substorms seems to be somewhat faster than that for weak substorms: Figure 3. This is not, however, conclusive; note that very fast tailward flows associated with the plasmoid can be observed even during weak auroral activities [*Ieda et al.*, 2001; *Ohtani et al.*, 2002a]. This is also the case with the earthward flow, although these events reported by *Ohtani et al.* [2002a, 2002b] are not fully developed substorms.

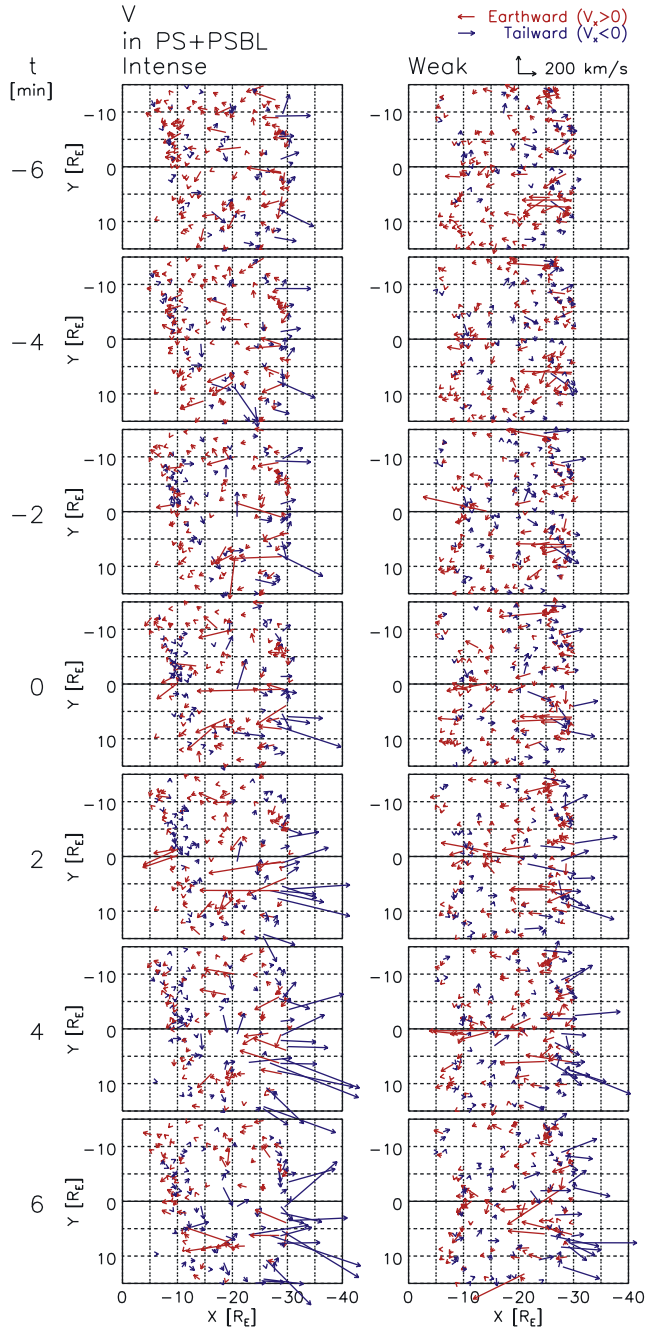

Figure 2. Variations in the plasma (ion) flows projected on the GSM X-Y plane in the plasma sheet (PS) and the plasma sheet boundary layer (PSBL) from $t = -6$ min to $t = 6$ min for (left) intense and (right) weak substorms. The times shown are for the centers of averaging intervals. The earthward ($V_x > 0$) and tailward ($V_x < 0$) flow vectors are plotted in red and blue, respectively. The scale of the vectors is indicated at the top.

[16] The Z component of the plasma flow (V_z) in the lobe and the PSBL is directed toward the PS before onset (not shown). It is enhanced in the entire tail after onset, associated with the plasmoid passage in the midtail region and the dipolarization at $X \sim -10\ R_E$. The enhancement at $X \sim -10\ R_E$ is more pronounced in intense substorms than in

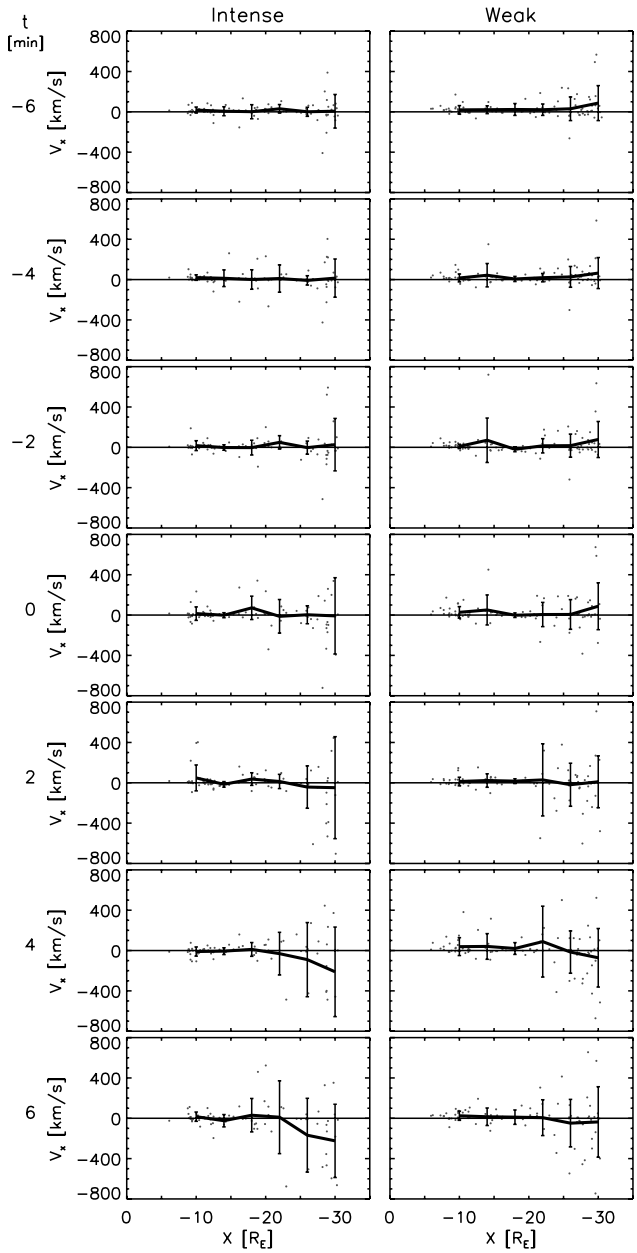

Figure 3. Sequential plot of the X-directional profile of the X component of the plasma flow (V_x) for (left) intense and (right) weak substorms. The dots indicate the 2-min values of V_x in the PS and PSBL of $X \leq -5\ R_E$ and $-3 \leq Y \leq 12\ R_E$. The thick lines and the error bars indicate the averages and the standard deviations, respectively, in 4 R_E bins in X.

weak substorms, while it does not differ very much in the midtail region between the two groups.

3.2. North-South Magnetic Field

[17] Figure 4 shows the deviations of the north-south magnetic field, $\Delta B_z(t) = B_z(t) - \overline{B_z}(t = -11 \sim -7$ min), in the PS, PSBL, and lobe, where $\overline{B_z}$ was defined as the average value over the interval from $t = -11$ min to $t = -7$ min, calculated for each event. Only the data satisfying $B_z \cdot \Delta B_z > 0$ are plotted in an attempt to exclude such variations as the magnetic field line stretching during the growth phase and to pick only the changes associated with substorm onset, such as the plasmoid/the traveling compression region (TCR) (growing southward B_z) and the dipolarization (growing northward B_z). Note that B_z is negative (positive) in the case of the negative (positive) ΔB_z. Figure 5 shows a sequential plot of the X-directional

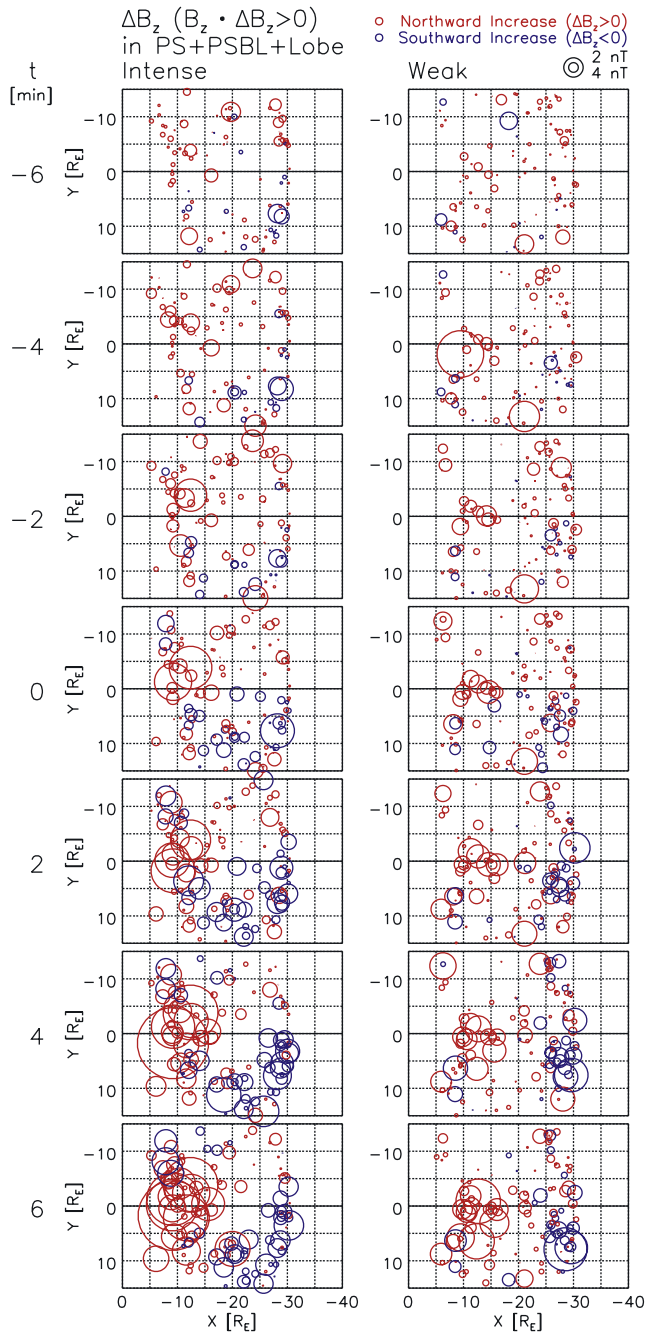

Figure 4. Variations in the deviations of the north-south magnetic field, i.e., $\Delta B_z(t) = B_z(t) - \overline{B_z}(t = -11 \sim -7$ min), in the PS, PSBL, and lobe, where $\overline{B_z}$ was defined as the average value over the interval from $t = -11$ min to $t = -7$ min, calculated for each event. Only the data satisfying $B_z \cdot \Delta B_z > 0$ are plotted. The positive and negative ΔB_z, i.e., northward and southward increases, are shown by red and blue circles, respectively, whose radii are proportional to the magnitude as indicated at the top.

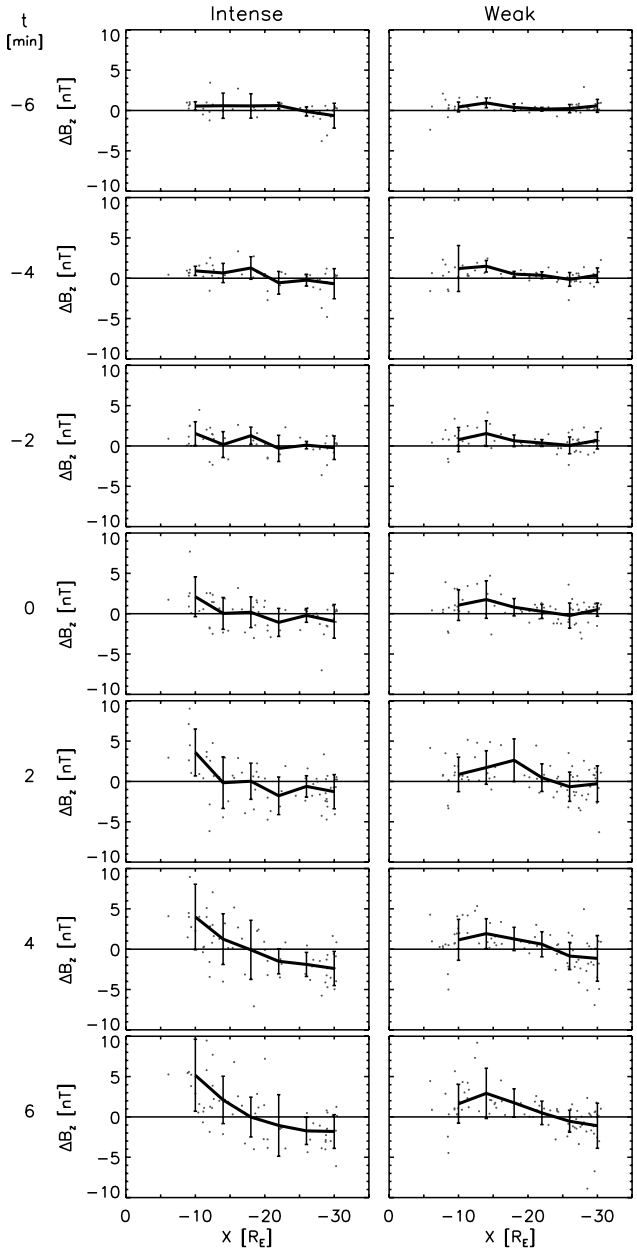

Figure 5. Sequential plot of the X-directional profile of the deviation of the north-south magnetic field (ΔB_z) satisfying $B_z \cdot \Delta B_z > 0$ in the PS, PSBL, and lobe of $X \leq -5\ R_E$ and $-3 \leq Y \leq 12\ R_E$ in the same format as Figure 3.

profile of ΔB_z satisfying $B_z \cdot \Delta B_z > 0$ in the PS, PSBL, and lobe of $X \leq -5\ R_E$ and $-3 \leq Y \leq 12\ R_E$.

[18] It is noticeable from Figures 4 and 5 that at onset more negative ΔB_z begins to appear and subsequently grow, i.e., B_z begins to become more southward in the premidnight sector of the midtail region, corresponding to the plasmoid in the PS or the TCR in the PSBL and the lobe. Most of the negative ΔB_z events are located tailward of $X \sim -17\ R_E$ for intense substorms, and tailward of $X \sim -23\ R_E$ for weak substorms. Also, the magnitude of the negative ΔB_z seems to be slightly larger for intense substorms.

[19] On the other hand, simultaneously with the plasmoid evolution, the positive ΔB_z begins to increase, i.e., the northward B_z increases at $X \sim -10\ R_E$ after $t \sim 0$ in association with the dipolarization. The development of the positive ΔB_z is more pronounced for intense substorms, in agreement with what the previous studies showed [*Kokubun and McPherron*, 1981; *Lui et al.*, 1992; *Lopez and von Rosenvinge*, 1993]. It seems likely that the positive ΔB_z is distributed to larger distances, i.e., the tailward boundary of the dipolarization region is located at larger distances for weak substorms. On the other hand, the location of the earthward boundary of the positive ΔB_z region or the dipolarization region does not appear to differ between the two groups. However, this is by no means definite since Geotail does not cover the region near geosynchronous orbit due to its perigee of $\sim 9\ R_E$.

[20] We also examined B_z itself, as shown in Figure 6. Before onset B_z is $\sim$10 nT at $X \sim -10\ R_E$ and rapidly decreases with increasing distance from the Earth for both groups. It becomes almost constant tailward of $X \sim -17\ R_E$ and $X \sim -22\ R_E$ for intense and weak substorms, respectively, implying that the magnetic field line is more stretched during intense substorms. The northward B_z tends to develop more significantly during intense substorms, associated with the dipolarization at $X \sim -10\ R_E$, while the negative B_z in the midtail region does not differ appreciably between the two groups.

3.3. Total Pressure

[21] We examined the normalized deviations of the total pressure, $\Delta P_t/\overline{P_t}(t = -11 \sim -7$ min), in the PS, PSBL, and lobe regions, where $\Delta P_t(t) = P_t(t) - \overline{P_t}(t = -11 \sim -7$ min). The total pressure is the sum of the ion and magnetic pressures, $P_t = NkT + B^2/2\mu_0$, where the contribution from electrons was neglected as well as that from high-energy particles beyond the instrumental range of Geotail LEP ($>\sim$40 keV/q). Here the results of the superposed epoch analysis in 4 R_E bins in X are shown in Figure 7, instead of the two-dimensional plots such as Figure 4. The Y range is $-3 \leq Y \leq 12\ R_E$ because of the dawn-dusk asymmetry of the magnetotail variations. Figure 8 shows a sequential plot of the X-directional profile of $\Delta P_t/\overline{P_t}$ in the same format as Figure 3.

[22] At $t \leq -4$ min, $\Delta P_t/\overline{P_t}$ is enhanced, i.e., the total pressure increases in the entire tail. The enhancement is more pronounced for more intense substorms. From $t = -2$ to 0 min, the total pressure begins to decrease first between $X = -10$ to $-18\ R_E$ for intense substorms, and between $X = -14$ to $-26\ R_E$ for weak substorms; the location of the first total pressure decrease tends to be closer to the Earth for intense substorms. Then, a total pressure decrease occurs in the surrounding regions successively. This total pressure decrease in these midtail regions relates to the magnetic reconnection [e.g., *Miyashita et al.*, 1999, 2000]. The total pressure also decreases at $X \sim -10\ R_E$ during the dipolarization, as shown by *Lyons et al.* [2003], although there are a few cases in which the total pressure continues to increase or decrease throughout the interval in this region. From Figure 7 the amount of the decrease in $\Delta P_t/\overline{P_t}$ is slightly larger in the entire tail for intense substorms than for weak substorms, which is consistent with the results of *Miyashita et al.* [2003a].

[23] Figure 9 shows a sequential plot of the X-directional profile of the total pressure itself (P_t). It is clearly seen that

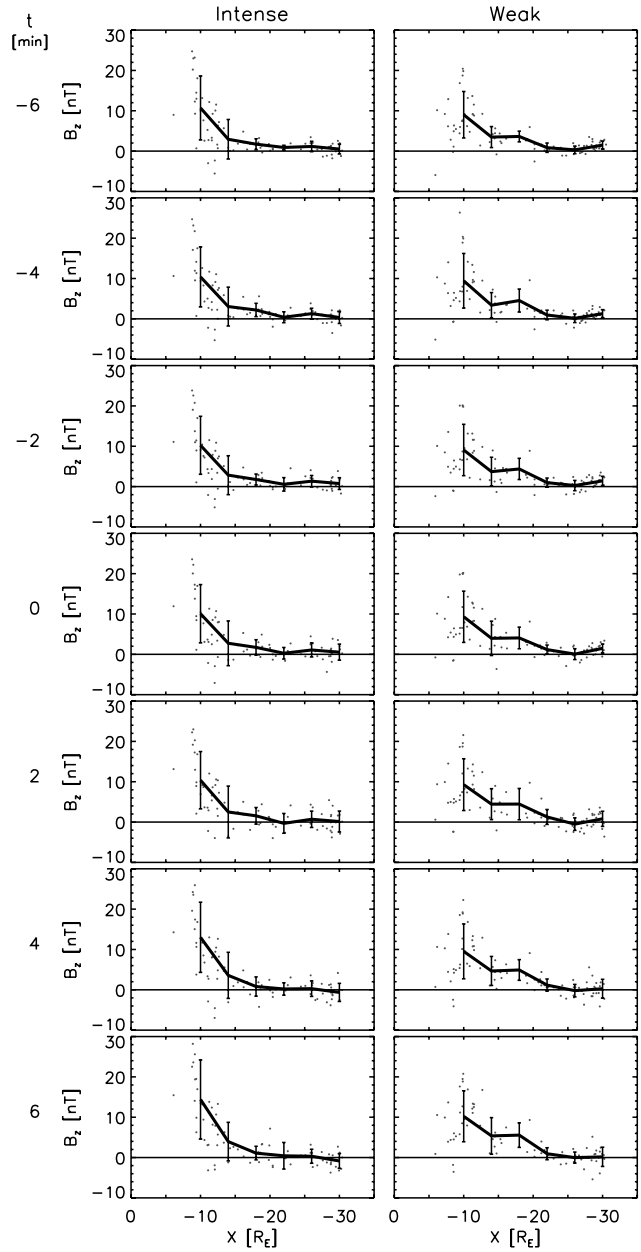

Figure 6. Sequential plot of the X-directional profile of the north-south magnetic field (B_z) in the PS and PSBL of $X \leq -5\ R_E$ and $-3 \leq Y \leq 12\ R_E$ in the same format as Figure 3.

the total pressure becomes larger on approaching the Earth. Comparing the total pressure for intense and weak substorms, the total pressure earthward of $X \sim -20\ R_E$ is larger throughout the interval for intense substorms than for weak substorms by a factor of $\sim$1–2, while the total pressure tailward of $X \sim -20\ R_E$ does not differ very much between the two groups. From the results of $\Delta P_t/\overline{P_t}$ and P_t, the substorm-associated decrease in the total pressure itself is larger at $X \sim -10\ R_E$ than in the midtail region, and it is larger in intense substorms than in weak substorms. These results are consistent with *Yamaguchi et al.* [2004].

3.4. Energy Fluxes

[24] We also examined the energy fluxes: the Poynting (electromagnetic) flux ($\mathbf{E} \times \mathbf{B}/\mu_0$), the kinetic (bulk) energy flux ($\rho V^2\mathbf{V}/2$), and the thermal (enthalpy) flux ($5P\mathbf{V}/2$). As shown by *Machida et al.* [2000] and *Miyashita et al.* [2001, 2003b], energy is provided from the lobe to the PS in the form of the Poynting flux, transported both tailward and earthward in the PS mainly in the form of the thermal flux. Hence we show here only the Z component of the Poynting flux in the lobe and PSBL and the thermal flux in the PS and PSBL.

[25] Figure 10 shows a sequential plot of the Z component of the Poynting flux in the lobe and PSBL. This results from the net transport distinct from the Poynting flux associated with electromagnetic waves. When we calculated the Poynting flux, we referred to the electric field calculated from the ion velocity and the magnetic field according to the frozen-in condition $\mathbf{E} = -\mathbf{V} \times \mathbf{B}$, because the Z component of the electric field was not directly measured by the double probe of the electric field detector (EFD) onboard Geotail [*Tsuruda et al.*, 1994]. In addition to the difficulty in measuring the electric field in the tenuous lobe by the probe technique, the X and Y components can include offsets due to the photoelectrons emitted from the spacecraft in sunlight, such that special care is required to subtract the offsets properly.

[26] It is evident that the Poynting flux toward the PS is several times larger at $X \sim -10\ R_E$ than at larger distances, because of the larger magnetic field at $X \sim -10\ R_E$. The flux is particularly larger at $X \sim -10\ R_E$ for intense substorms than for weak substorms, while it is not different very much at larger distances in the two groups. At expansion onset, the Poynting flux toward the PS starts to increase in the entire tail, especially at $X \sim -10\ R_E$, in conjunction with the plasmoid passage at $-20 > X > -30\ R_E$ and the dipolarization at $X \sim -10\ R_E$. The enhancement at $X \sim -10\ R_E$ is more pronounced in intense substorms than in weak substorms, but that at larger distances does not differ between the two groups. Similar enhancements are seen in the plasma flow toward the PS and the dawn-dusk electric field in the lobe and the PSBL, reflecting the frozen-in condition.

[27] Figure 11 shows a sequential plot of the X component of the thermal flux in the PS and PSBL, where we assumed isotropic and adiabatic plasmas. We considered the contribution only from ions, neglecting that from electrons as well as from high-energy particles beyond the instrumental range of Geotail LEP ($>\sim$40 keV/q). After expansion onset, tailward thermal fluxes develop significantly in the premidnight sector of $-25 > X > -30\ R_E$, associated with the plasmoid. Simultaneously with this development, earthward thermal fluxes also become large at $X \sim -10\ R_E$. These fluxes may relate to the dipolarization process or may be generated at larger distances. A few of these earthward thermal fluxes for intense substorms are very large, much larger than the upper limit of Figure 11. Both tailward and earthward thermal fluxes after onset may be larger for intense substorms than for weak substorms.

4. Discussion

[28] The statistical results shown in the present paper demonstrate that the southward magnetic field associated with the plasmoid and the TCR dominates tailward of $X \sim -17\ R_E$ and $X \sim -23\ R_E$ for intense and weak substorms,

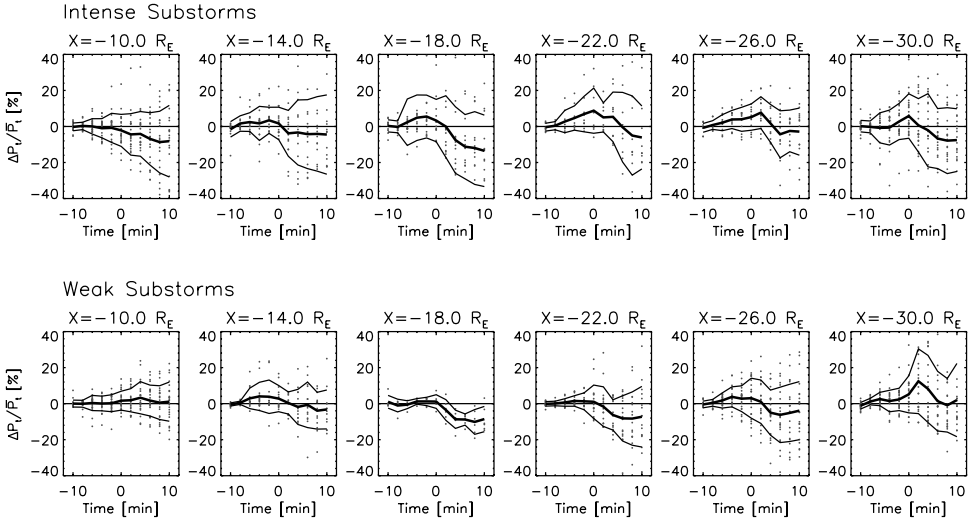

Figure 7. Results of the superposed epoch analysis in 4 R_E bins in X for the normalized total pressure deviations ($\Delta P_t/\overline{P_t}$) in the PS, PSBL, and lobe of $-3 \leq Y \leq 12$ R_E for (top) intense and (bottom) weak substorms. The deviation ΔP_t was defined for each event as $\Delta P_t(t) = P_t(t) - \overline{P_t}(t = -11 \sim -7$ min). In each panel the center of the bin is shown at the top. The thick line indicates the average, whereas the top (bottom) thin line indicates the sum (difference) of the average and the standard deviation.

respectively. Also, the first total pressure decrease, which is related to the magnetic reconnection, tends to occur closer to the Earth for intense substorms than for weak substorms, i.e., at $X \sim -14$ R_E and $X \sim -20$ R_E for intense and weak substorms, respectively. Fast tailward flows associated with plasmoids are hardly observed earthward of $X \sim -20$ R_E. This is probably because the very thin plasma sheet extends from the near-Earth tail to $X \sim -20$ R_E, so that it can be easy to miss the fast flows earthward of $X \sim -20$ R_E. On the basis of the observational results of the southward magnetic field and the total pressure, we conclude that the location of the first energy release, or the magnetic reconnection site at onset, is closer to the Earth for intense substorms than for weak substorms, i.e., at $X \sim -14$ to -17 R_E for intense substorms, and at $X \sim -20$ to -23 R_E for weak substorms.

[29] The onset latitude in the ionosphere depends on the substorm intensity, as noted in the Introduction. The location of the initial brightening maps to the near-Earth magnetosphere, $\sim$6–10 R_E [e.g., *Samson et al.*, 1992], which corresponds to the dipolarization region at onset. That is, the location of the first dipolarization is expected to depend directly on the substorm intensity. Here it should be noted that the dependence of the dipolarization region cannot be observed by Geotail, since it does not cover the region near geosynchronous orbit due to the spacecraft's perigee, $\sim$9 R_E. On the other hand, the magnetic reconnection site does not map to the initial brightening, but the location of the magnetic reconnection site also varies according to the substorm intensity, as shown in the present study.

[30] The magnetotail variations associated with expansion onset were shown not to differ morphologically between intense and weak substorms, although the absolute values and the deviations of the parameters tend to be larger for intense substorms. The timing of the beginning of the substorm-associated variation also seems to be common in 2 min time resolution between the two groups. The timing is expected to depend on the substorm intensity, since the location of the magnetic reconnection site differs by several R_E between intense and weak substorms. That is, the propagation time of the information on the magnetic reconnection occurrence to the ionosphere can be shorter for intense substorms than for weak substorms. The difference in the propagation time between the two groups, however, may be so slight that it is smeared out in the 2 min resolution.

[31] As shown in Figure 6, the radial gradient of B_z becomes very small at $X \sim -17$ R_E and $X \sim -22$ R_E for intense and weak substorms, respectively. This implies that the magnetic field lines are more stretched and the thin current sheet develops more efficiently for intense substorms. The thin current sheet may extend from the near-Earth tail to these regions. From our results, these regions roughly agree with the possible location of the magnetic reconnection site. This is consistent with the results of *Asano et al.* [2004], who proposed that the magnetic reconnection occurs near the tailward edge of the thin current sheet. As discussed by *Miyashita et al.* [2003b], the effects of the northward B_z and the asymmetry in the X direction on the magnetic reconnection may be important to understand the substorm triggering mechanism.

[32] The absolute values of the total pressure and the Poynting flux toward the PS in the lobe increase with decreasing distance from the Earth. These values at $X \sim -10$ R_E are larger for intense substorms than for weak substorms, while those in the midtail region do not differ very much between the two groups. The enhancement of the Poynting flux toward the PS and the decrease in the total pressure at expansion onset are more pronounced at $X \sim -10$ R_E in intense substorms, while these variations in the midtail region do not depend very much on the substorm intensity. From these results, it is understood that significant portions of the energy required for a substorm are accumulated in the near-Earth region rather than in the midtail region, probably being subsequently dissipated by the process of the current disruption or the dipolarization

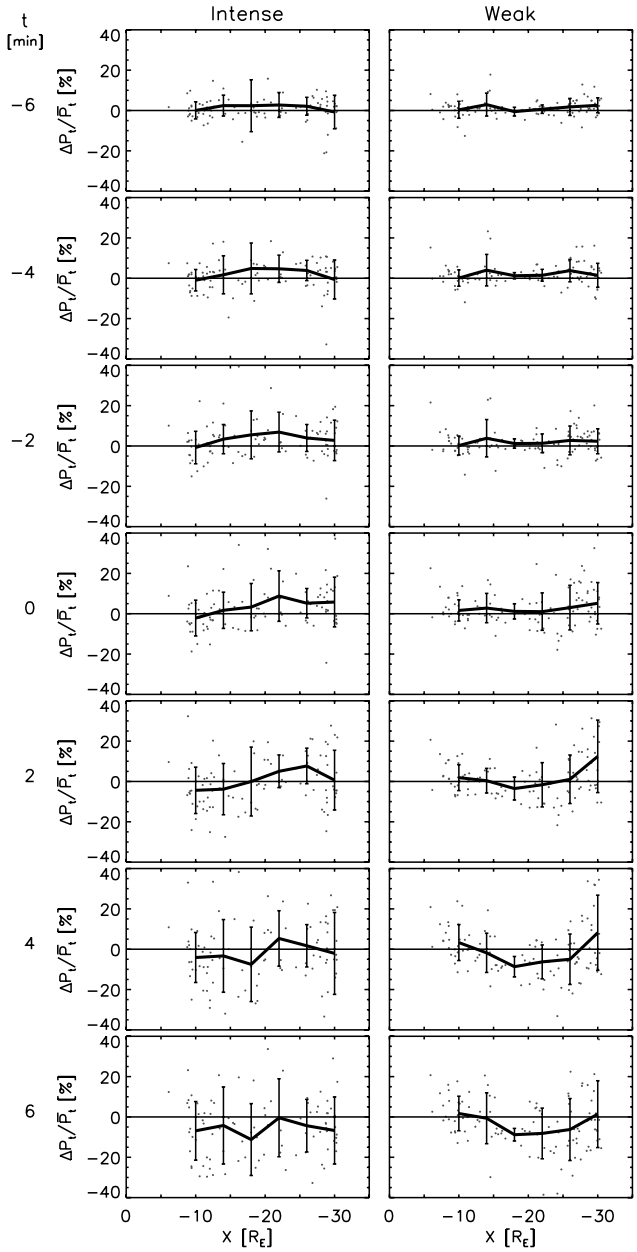

Figure 8. Sequential plot of the X-directional profile of the normalized total pressure deviation ($\Delta P_t/\overline{P_t}$) in the PS, PSBL, and lobe of $X \leq -5\ R_E$ and $-3 \leq Y \leq 12\ R_E$ in the same format as Figure 3.

triggered by the magnetic reconnection, and naturally that the amount of the energy is larger for intense substorms than for weak substorms.

[33] One of the unsolved issues is why a substorm can grow intense or what determines the substorm intensity. From our results of the total pressure and the Poynting flux, we propose that energy input and output is one of the controlling factors in the substorm intensity. That is, more energy is provided and stored mainly in the near-Earth region and is subsequently released at expansion onset in more intense substorms. *Miyashita et al.* [2003a] showed that the total pressure has a larger decrease in intense substorms, although they examined mainly events that were observed tailward of the magnetic reconnection site. Another controlling factor can be continuous solar wind input after the expansion onset [*Pulkkinen et al.*, 1998; *Kallio et al.*, 2000]. Furthermore, a longer duration of the expansion phase may result in a more intense substorm, even if a rate of energy release is not very high.

[34] On the other hand, it is of course important to understand properly what conditions are required for the substorm triggering. Regardless of the substorm intensity, some substorms seem to occur even in the course of energy accumulation in the magnetotail, while some other substorms do not seem to be triggered effectively in spite of continuous energy accumulation. Conditions other than the amount of stored energy in the magnetotail can be necessary

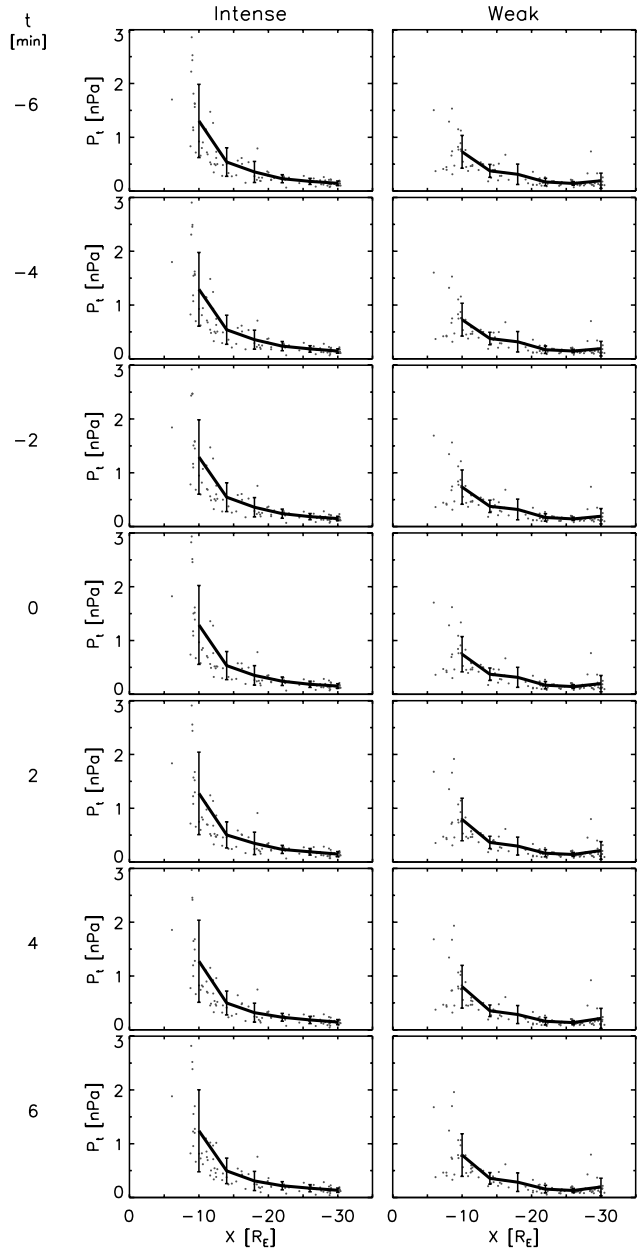

Figure 9. Sequential plot of the X-directional profile of the total pressure (P_t) in the PS, PSBL, and lobe of $X \leq -5\ R_E$ and $-3 \leq Y \leq 12\ R_E$ in the same format as Figure 3.

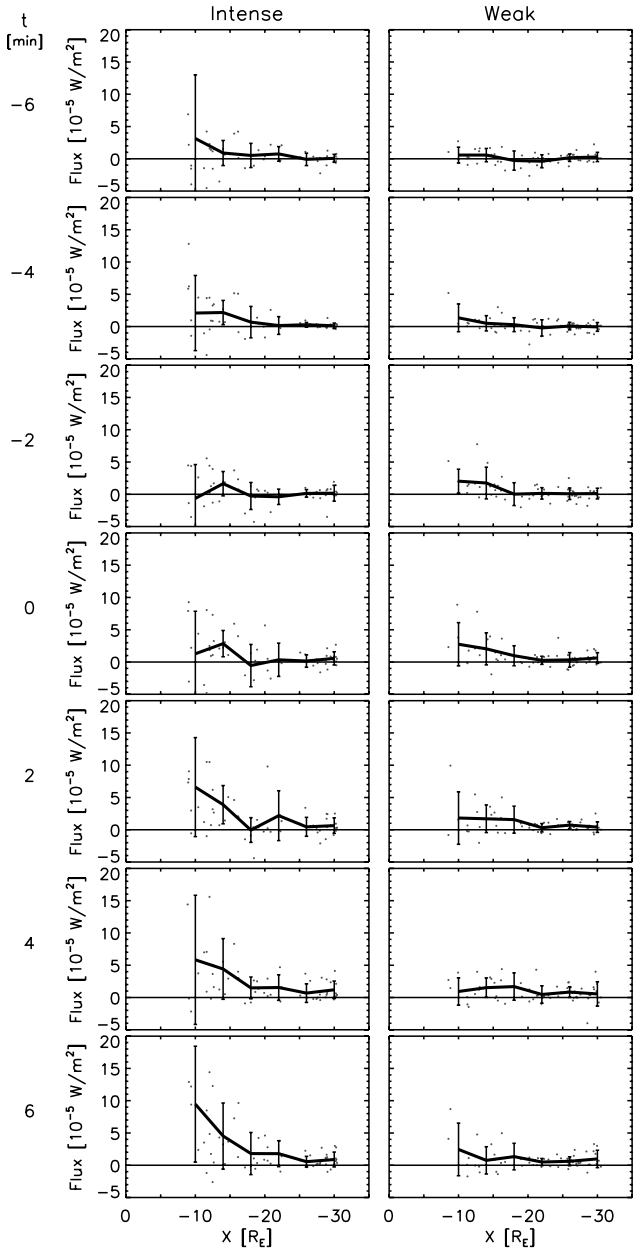

Figure 10. Sequential plot of the X-directional profile of the Z component of the Poynting flux in the lobe and PSBL of $X \leq -5\ R_E$ and $-3 \leq Y \leq 12\ R_E$ in the same format as Figure 3. The positive (negative) component is directed toward the PS (lobe).

for the substorm triggering, but this problem is an open question.

[35] We did not classify the substorm events according to storm time or nonstorm time in the present study. *Baumjohann et al.* [1996] speculated from their analysis of AMPTE IRM data at $10 < R < 19\ R_E$ that storm time and nonstorm time substorms are caused by different mechanisms. *McPherron and Hsu* [2002] suggested, however, from ISEE 2 data at $R < 23\ R_E$ that both types of substorms are caused by the same mechanism. In our preliminary study, we have divided our substorm events into storm time and nonstorm time substorms. We found that there is no qualitative difference between storm time and nonstorm time substorms in terms of the occurrence of the magnetic reconnection and the dipolarization in the magnetotail, suggesting that both substorms are caused by the same mechanism. This result will be reported in a future paper.

5. Conclusions

[36] Using Geotail data, we statistically studied the difference in substorm-associated variations in the magnetotail between intense and weak substorms. For intense substorms, the regime of the southward magnetic field associated with the plasmoid was shown to extend closer to the

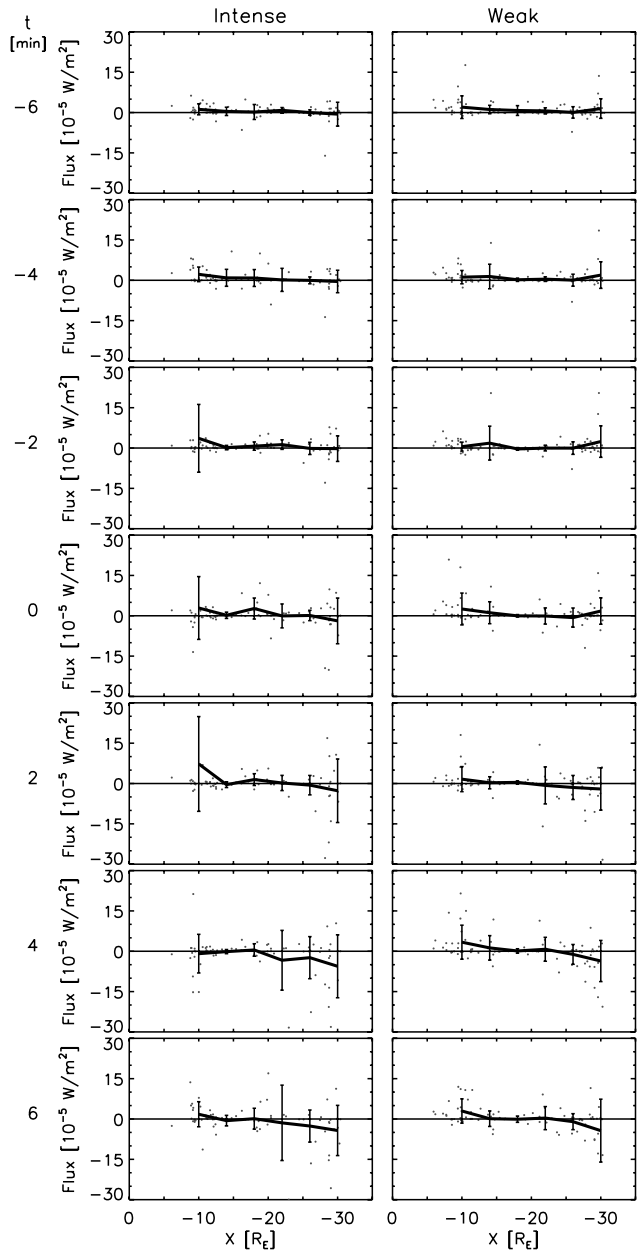

Figure 11. Sequential plot of the X-directional profile of the X component of the thermal flux in the PS and PSBL of $X \leq -5\ R_E$ and $-3 \leq Y \leq 12\ R_E$ in the same format as Figure 3.

Earth. The first indication of the total pressure decrease also occurs closer to the Earth. These results suggest that the magnetic reconnection site at onset is located closer to the Earth in intense substorms. This tendency is consistent with the latitudinal dependence of the onset location in the ionosphere. Also, magnetic field lines during the growth phase especially earthward of the magnetic reconnection site are more stretched in intense substorms than in weak substorms. The magnetic reconnection seems to occur near the region where the radial gradient of the northward magnetic field becomes small. The dipolarization at $X \sim -10\ R_E$ is more significant in intense substorms. Furthermore, the Poynting flux toward the plasma sheet in the lobe and the total pressure in the growth and expansion phases are larger at $X \sim -10\ R_E$ than at larger distances, and they are larger during intense substorms than during weak substorms. During the expansion phase, the Poynting flux is more enhanced, and the total pressure decrease is more pronounced at $X \sim -10\ R_E$ in intense substorms. These results suggest that more energy is accumulated and subsequently dissipated in the near-Earth magnetotail at $X \sim -10\ R_E$ for intense substorms.

[37] **Acknowledgments.** The Geotail MGF magnetic field data were provided by S. Kokubun and T. Nagai. The geomagnetic field data were provided by World Data Center for Geomagnetism, Kyoto. We thank T. Nagai for his useful comments. One of the authors (Y.M.) was supported in part by Research Fellowships of the Japan Society for the Promotion of Science for Young Scientists.

[38] Lou-Chuang Lee thanks Donald Fairfield and the other reviewer for their assistance in evaluating this article.

References

Asano, Y., T. Mukai, M. Hoshino, Y. Saito, H. Hayakawa, and T. Nagai (2004), Statistical study of thin current sheet evolution around substorm onset, *J. Geophys. Res.*, *109*, A05213, doi:10.1029/2004JA010413.

Baker, D. N., T. I. Pulkkinen, V. Angelopoulos, W. Baumjohann, and R. L. McPherron (1996), Neutral line model of substorms: Past results and present view, *J. Geophys. Res.*, *101*, 12,975–13,010.

Baumjohann, W., G. Paschmann, T. Nagai, and H. Lühr (1991), Superposed epoch analysis of the substorm plasma sheet, *J. Geophys. Res.*, *96*, 11,605–11,608.

Baumjohann, W., Y. Kamide, and R. Nakamura (1996), Substorms, storms, and the near-Earth tail, *J. Geomagn. Geoelectr.*, *48*, 177–185.

Baumjohann, W., M. Hesse, S. Kokubun, T. Mukai, T. Nagai, and A. A. Petrukovich (1999), Substorm dipolarization and recovery, *J. Geophys. Res.*, *104*, 24,995–25,000.

Hones, E. W., Jr. (1976), The magnetotail: Its generation and dissipation, in *Physics of Solar Planetary Environments*, edited by D. J. Williams, pp. 558–571, AGU, Washington, D. C.

Ieda, A., S. Machida, T. Mukai, Y. Saito, T. Yamamoto, A. Nishida, T. Terasawa, and S. Kokubun (1998), Statistical analysis of the plasmoid evolution with Geotail observations, *J. Geophys. Res.*, *103*, 4453–4465.

Ieda, A., D. H. Fairfield, T. Mukai, Y. Saito, S. Kokubun, K. Liou, C.-I. Meng, G. K. Parks, and M. J. Brittnacher (2001), Plasmoid ejection and auroral brightenings, *J. Geophys. Res.*, *106*, 3845–3857.

Kallio, E. I., T. I. Pulkkinen, H. E. J. Koskinen, A. Viljanen, J. A. Slavin, and K. Ogilvie (2000), Loading-unloading processes in the nightside ionosphere, *Geophys. Res. Lett.*, *27*, 1627–1630.

Kamide, Y. (1970), Spatial extent of the return current of the auroral-zone electrojet, Part III, *Rep. Ionos. Space Res. Jpn.*, *24*, 347–352.

Kamide, Y. (2001), Some "missing" elements of constraint in substorm initiation modeling, *J. Atmos. Sol. Terr. Phys.*, *63*, 635–642.

Kamide, Y., and S.-I. Akasofu (1974), Latitudinal cross section of the auroral electrojet and its relation to the interplanetary magnetic field polarity, *J. Geophys. Res.*, *79*, 3755–3771.

Kamide, Y., F. Yasuhara, and S.-I. Akasofu (1974), On the cause of northward magnetic field along the negative X axis during magnetospheric substorms, *Planet. Space Sci.*, *22*, 1219–1229.

Kokubun, S., and R. L. McPherron (1981), Substorm signatures at synchronous altitude, *J. Geophys. Res.*, *86*, 11,265–11,277.

Kokubun, S., T. Yamamoto, M. H. Acuña, K. Hayashi, K. Shiokawa, and H. Kawano (1994), The Geotail magnetic field experiment, *J. Geomagn. Geoelectr.*, *46*, 7–21.

Liou, K., C.-I. Meng, A. T. Y. Lui, P. T. Newell, M. Brittnacher, G. Parks, G. D. Reeves, R. R. Anderson, and K. Yumoto (1999), On relative timing in substorm onset signatures, *J. Geophys. Res.*, *104*, 22,807–22,817.

Liou, K., C.-I. Meng, P. T. Newell, K. Takahashi, S.-I. Ohtani, A. T. Y. Lui, M. Brittnacher, and G. Parks (2000), Evaluation of low-latitude Pi2 pulsations as indicators of substorm onset using Polar ultraviolet imagery, *J. Geophys. Res.*, *105*, 2495–2505.

Lopez, R. E., and T. von Rosenvinge (1993), A statistical relationship between the geosynchronous magnetic field and substorm electrojet magnitude, *J. Geophys. Res.*, *98*, 3851–3857.

Lui, A. T. Y. (1993), What determines the intensity of magnetospheric substorms?, *J. Atmos. Terr. Phys.*, *55*, 1123–1136.

Lui, A. T. Y. (1996), Current disruption in the Earth's magnetosphere: Observations and models, *J. Geophys. Res.*, *101*, 13,067–13,088.

Lui, A. T. Y., A. Mankofsky, C.-L. Chang, K. Papadopoulos, and C. S. Wu (1990), A current disruption mechanism in the neutral sheet: A possible trigger for substorm expansions, *Geophys. Res. Lett.*, *17*, 745–748.

Lui, A. T. Y., R. E. Lopez, B. J. Anderson, K. Takahashi, L. J. Zanetti, R. W. McEntire, T. A. Potemra, D. M. Klumpar, E. M. Greene, and R. Strangeway (1992), Current disruptions in the near-Earth neutral sheet region, *J. Geophys. Res.*, *97*, 1461–1480.

Lui, A. T. Y., K. Liou, P. T. Newell, C.-I. Meng, S.-I. Ohtani, T. Ogino, S. Kokubun, M. J. Brittnacher, and G. K. Parks (1998), Plasma and magnetic flux transport associated with auroral breakups, *Geophys. Res. Lett.*, *25*, 4059–4062.

Lyons, L. R., C.-P. Wang, T. Nagai, T. Mukai, Y. Saito, and J. C. Samson (2003), Substorm inner plasma sheet particle reduction, *J. Geophys. Res.*, *108*(A12), 1426, doi:10.1029/2003JA010177.

Machida, S., Y. Miyashita, A. Ieda, A. Nishida, T. Mukai, Y. Saito, and S. Kokubun (1999), Geotail observations of flow velocity and north-south magnetic field variations in the near and mid-distant tail associated with substorm onsets, *Geophys. Res. Lett.*, *26*, 635–638.

Machida, S., A. Ieda, T. Mukai, Y. Saito, and A. Nishida (2000), Statistical visualization of the Earth's magnetotail during substorms by means of multidimensional superposed epoch analysis with Geotail data, *J. Geophys. Res.*, *105*, 25,291–25,303.

McPherron, R. L., and D. N. Baker (1993), Factors influencing the intensity of magnetospheric substorms, *J. Atmos. Terr. Phys.*, *55*, 1091–1122.

McPherron, R. L., and T.-S. Hsu (2002), A comparison of substorms occurring during magnetic storms with those occurring during quiet times, *J. Geophys. Res.*, *107*(A9), 1259, doi:10.1029/2001JA002008.

Miyashita, Y., S. Machida, A. Nishida, T. Mukai, Y. Saito, and S. Kokubun (1999), Geotail observations of total pressure and electric field variations in the near and mid-distant tail associated with substorm onsets, *Geophys. Res. Lett.*, *26*, 639–642.

Miyashita, Y., S. Machida, T. Mukai, Y. Saito, K. Tsuruda, H. Hayakawa, and P. R. Sutcliffe (2000), A statistical study of variations in the near and middistant magnetotail associated with substorm onsets: Geotail observations, *J. Geophys. Res.*, *105*, 15,913–15,930.

Miyashita, Y., S. Machida, T. Mukai, Y. Saito, and P. R. Sutcliffe (2001), Mass and energy transport in the near and middistant magnetotail around substorm onsets: Geotail observations, *J. Geophys. Res.*, *106*, 6259–6274.

Miyashita, Y., S. Machida, K. Liou, T. Mukai, Y. Saito, C.-I. Meng, and G. K. Parks (2003a), Relationship between magnetotail variations and auroral activities during substorms, *J. Geophys. Res.*, *108*(A1), 1022, doi:10.1029/2001JA009175.

Miyashita, Y., S. Machida, K. Liou, T. Mukai, Y. Saito, H. Hayakawa, C.-I. Meng, and G. K. Parks (2003b), Evolution of the magnetotail associated with substorm auroral breakups, *J. Geophys. Res.*, *108*(A9), 1353, doi:10.1029/2003JA009939.

Mukai, T., S. Machida, Y. Saito, M. Hirahara, T. Terasawa, N. Kaya, T. Obara, M. Ejiri, and A. Nishida (1994), The low energy particle (LEP) experiment onboard the Geotail satellite, *J. Geomagn. Geoelectr.*, *46*, 669–692.

Nagai, T., M. Fujimoto, Y. Saito, S. Machida, T. Terasawa, R. Nakamura, T. Yamamoto, T. Mukai, A. Nishida, and S. Kokubun (1998), Structure and dynamics of magnetic reconnection for substorm onsets with Geotail observations, *J. Geophys. Res.*, *103*, 4419–4440.

Ohtani, S., R. Yamaguchi, M. Nosé, H. Kawano, M. Engebretson, and K. Yumoto (2002a), Quiet time magnetotail dynamics and their implications for the substorm trigger, *J. Geophys. Res.*, *107*(A2), 1030, doi:10.1029/2001JA000116.

Ohtani, S., R. Yamaguchi, H. Kawano, F. Creutzberg, J. B. Sigwarth, L. A. Frank, and T. Mukai (2002b), Does the braking of the fast plasma flow trigger a substorm?: A study of the August 14, 1996, event, *Geophys. Res. Lett.*, *29*(15), 1721, doi:10.1029/2001GL013785.

Pulkkinen, T. I., D. N. Baker, L. L. Cogger, T. Mukai, and H. J. Singer (1998), Coupling of inner tail and midtail processes, in *Proceedings of International Conference on Substorms-4*, edited by S. Kokubun and Y. Kamide, pp. 749–754, Terra Sci., Tokyo.

Roux, A., S. Perraut, P. Robert, A. Morane, A. Pedersen, A. Korth, G. Kremser, B. Aparicio, D. Rodgers, and R. Pellinen (1991), Plasma sheet instability related to the westward traveling surge, *J. Geophys. Res.*, *96*, 17,697–17,714.

Samson, J. C., L. R. Lyons, P. T. Newell, F. Creutzberg, and B. Xu (1992), Proton aurora and substorm intensifications, *Geophys. Res. Lett.*, *19*, 2167–2170.

Torr, M. R., et al. (1995), A far ultraviolet imager for the international solar-terrestrial physics mission, *Space Sci. Rev.*, *71*, 329–383.

Tsuruda, K., H. Hayakawa, M. Nakamura, T. Okada, A. Matsuoka, F. S. Mozer, and R. Schmidt (1994), Electric field measurements on the Geotail satellite, *J. Geomagn. Geoelectr.*, *46*, 693–711.

Yamaguchi, R., H. Kawano, S. Ohtani, S. Kokubun, and K. Yumoto (2004), Total pressure variations in the magnetotail as a function of the position and the substorm magnitude, *J. Geophys. Res.*, *109*, A03206, doi:10.1029/2003JA010196.

A. Ieda, Y. Kamide, and Y. Miyashita, Solar-Terrestrial Environment Laboratory, Nagoya University, Toyokawa, Aichi 442-8507, Japan. (ieda@stelab.nagoya-u.ac.jp; kamide@stelab.nagoya-u.ac.jp; miyasita@stelab.nagoya-u.ac.jp)

K. Liou and C.-I. Meng, Johns Hopkins University, Applied Physics Laboratory, Laurel, MD 20723, USA. (kan.liou@jhuapl.edu; ching.meng@jhuapl.edu)

S. Machida, Department of Geophysics, Kyoto University, Kyoto 606-8502, Japan. (machida@kugi.kyoto-u.ac.jp)

T. Mukai and Y. Saito, Institute of Space and Astronautical Science, Japan Aerospace Exploration Agency, Sagamihara, Kanagawa 229-8510, Japan. (mukai@stp.isas.jaxa.jp; saito@stp.isas.jaxa.jp)

G. K. Parks, Space Sciences Laboratory, University of California, Berkeley, CA 94720, USA. (parks@ssl.berkeley.edu)